The Evaporative Demand Drought Index: Part I – Linking Drought Evolution to Variations in Evaporative Demand

Michael Hobbins[1,2], Andrew Wood[3], Daniel McEvoy[4,5], Justin Huntington[4,5], and Charles Morton[5]

1. University of Colorado-Cooperative Institute for Research in Environmental Sciences, Boulder, CO
2. NOAA-Earth Systems Research Laboratory, Physical Sciences Division, Boulder, CO
3. National Center for Atmospheric Research, Boulder, CO
4. University of Nevada Reno, Reno, NV
5. Desert Research Institute, Reno, NV

Corresponding author: Michael Hobbins (mike.hobbins@noaa.gov)

Abstract

Many operational drought indices focus primarily on precipitation and temperature when depicting hydroclimatic anomalies, and this perspective can be augmented by analyses and products that reflect the evaporative dynamics of drought. We leverage the linkage between atmospheric evaporative demand (E_0) and actual evapotranspiration (ET) in a new drought index based on E_0—the Evaporative Demand Drought Index (EDDI). EDDI measures the signal of drought through the response of E_0 to surface drying anomalies that result from two distinct land surface-atmosphere interactions: (1) a complementary relationship between E_0 and ET that develops as moisture becomes limited at the land surface, leading to ET declining and increasing E_0, as in sustained droughts; and (2) parallel ET and E_0 increases arising from increased energy availability leading up to surface moisture limitation, as in flash droughts. To calculate EDDI from E_0, we use a long-term, daily reanalysis of reference ET (ET_0) estimated by the ASCE Standardized Reference ET equation using radiation and meteorological variables from the North American Land Data Assimilation System phase-2 (NLDAS). EDDI is derived by normalizing aggregated ET_0 anomalies from climatologic means across a user-specific time period. Positive EDDI values then indicate drier than normal conditions and the potential for drought. EDDI is thus a physically based, multi-scalar drought index that that can serve as an indicator of both flash and sustained droughts, in some cases offering early warning relative to current operational drought indices.

1. Introduction

Drought severely affects society, ecology, and economies, with impacts felt across sectors and hydrologic and political boundaries at time scales that vary from weeks to years. Physically, it is manifest as deficits in moisture fluxes and storages, including precipitation (Prcp) in meteorological drought; streamflow (Runoff) and surface storage depletion in hydrologic drought; and, traditionally, ET and soil moisture (SM) in agricultural drought. Agricultural and meteorological droughts are also evinced as a surplus in atmospheric evaporative demand (E_0, also sometimes referred to as "potential evaporation"). E_0 physically integrates radiative and advective forcing variabilities and, further, reflects water availability through land surface-atmosphere feedbacks. As such, it can serve as an independent drought indicator without conversion to ET through parameterizations of soil-water and plant-water availabilities that may be of questionable value on operational space and time scales.

The current iteration of the United States Drought Monitor (USDM) relies heavily on Prcp and air temperature (T_{air}) data to derive drought category assessments and other ancillary products such as surface moisture fluxes. E_0 is used only in implicit manner to derive ET fluxes through land surface models (LSMs), but is not an explicit input to the USDM. Further, nowhere in the USDM is E_0 directly used in a physically comprehensive format—i.e., one that integrates both radiative and advective drivers. Instead, simple formulations based on T_{air} alone are used: the Palmer Drought Severity Index (PDSI; Palmer 1965) employs a Thornthwaite-like T_{air}-based E_0 (Thornthwaite 1948); the "leaky bucket" CPC soil moisture model uses the T_{air}-based Hargreaves reference ET (Hargreaves and Samani 1985). However, the choice of E_0 formulation for bucket models significantly affects both the magnitude and direction of short- and long-term trends in estimated ET and SM, particularly in energy-limited areas. All else equal, T_{air}-based E_0 measures show declines in long-term ET (i.e., drying) as T_{air} rises (Dai et al. 2004)—in opposition to worldwide (and CONUS) observed trends (Hobbins et al. 2004; Roderick et al. 2009). Furthermore, a number of studies show that T_{air} is often not the most significant driver of long-term E_0 trends (e.g., Roderick et al. 2007). For example, while the short-term (daily) variability of E_0 during the critical growing season is dominated by T_{air} over most of CONUS, it is notably most strongly influenced by 2-m wind speed (U_2) in the southwest and downwelling shortwave radiation (R_d) in the southeast (Hobbins et al. 2012; Hobbins 2015). Arguably, more physically explicit E_0 formulations will more accurately reflect observations of both wetting and drying under warming (Hobbins et al. 2008; Sheffield et al. 2012).

Several emerging drought indices are predicated on the drought signal of physically based ET [e.g., the Soil Moisture Deficit Index (SMDI) and Evapotranspiration Deficit Index (ETDI) of Narasimhan and Srinivasan (2005); the Standardised Precipitation Evapotranspiration Index (SPEI) of Vicente-Serrano et al. (2010); the Evapotranspiration Stress Index (ESI) of Anderson et al. (2007); the Remotely Sensed Global Drought Severity Index of Mu et al. (2013); and the Optimal Blended NLDAS Drought Index of Xia et al. (2014)]. They generally rely on a combination of land-based and remotely sensed data and, as such, are data- and/or computationally intensive and can have significant latencies (e.g., due to inter-satellite overpass periods). However, while E_0 could be a flexible driver in drought monitoring—it may be remotely sensed, land-based, or physically observed, and it does not rely on LSMs—no existing indices relate to E_0 alone. An index based solely on a physically based E_0 measure has several advantages: characterization of the surface water availability is obviated, as are difficulties intrinsic to remotely sensed data streams such as delays and the requisite infilling of data due to satellite-overpass intervals or cloud cover. Such an index could help fill a gap between science and applications, in that it is operationally tractable for detecting and monitoring both flash and sustained droughts, with negligible latency.

Depending on whether ET is limited by the availability of energy or of water, E_0 either plays a role in determining ET or else is reflective of ET. In non-water limited conditions, E_0 estimates the upper limit of (energy-limited) ET, whereas in water-limited conditions, land-atmosphere feedbacks generated from ET force in E_0 in a complementary direction. Clearly, in sustained drought (i.e., sustained deficits in SM and associated fluxes at the land-atmosphere interface), the water limit applies to ET. This is less often true, however, in the case of "flash drought" (i.e., a fast-developing drought driven by strong, transient increases in T_{air}, humidity, wind, or radiation) with no substantive change in Prcp). Nonetheless, the positive E_0 signal manifested in both sustained and flash droughts suggests that E_0 has value both for monitoring droughts and as a leading indicator of developing drought conditions.

In this paper, we offer a physical rationale for an E_0-based drought index and propose an index formulation, termed the Evaporative Demand Drought Index (EDDI). The performance of EDDI is assessed across CONUS in a companion paper (McEvoy et al. - this issue). This paper develops the theoretical basis of EDDI and demonstrates how the E_0 connection to drought makes it not only a useful drought metric but also provides for drought attribution by providing a decomposition of drought evolution to its separate meteorological forcings. We compare EDDI with drought indices based on ET and the USDM in case studies of flash and sustained droughts, in basins drawn from across CONUS's hydroclimatic spectrum (see Figure 1). We also examine EDDI's long-term performance as a leading drought indicator, and close with discussion and conclusions that motivate the companion paper (McEvoy et al. - this issue).

< Figure 1 here >

2. Physical rationale for E_0-based drought indicator

The complementary and parallel interactions of ET and E_0 in both sustained and flash droughts form the physical basis for EDDI. Drought links to E_0 from one of two dynamics, depending on the prevailing hydroclimate. In the first, under moist, energy-limited ET conditions, variations in surface energy Q_n (the sum of the fluxes of sensible heat H and latent heat λET to the atmosphere) cause both ET and E_0 to vary proportionally to Q_n. Second, under water-limited ET conditions, variability in ET drives a complementary variability in E_0 through energetic interactions across the land-atmosphere interface. This is known as the "complementary relationship" (Bouchet 1963): when ET becomes water-limited, Q_n is re-partitioned to favor sensible heat H over λET. The increased H raises the vapor pressure deficit of the dynamic boundary layer and thereby increases E_0. In its simplest expression:

$$ET = kE_w - E_0 \tag{1}$$

where E_w is the ET rate for a regional-scale wet surface. Often, k is assumed to be 2, implying that the energy released at the surface by declining λET is reapportioned to H and raises E_0 by as much as λET falls. Others have shown that k may fall into the range 2-5 [e.g., Pettijohn and Salvucci (2009); Szilagyi (2007)], but the particular value of k is not functionally important to the performance of EDDI. Figure 2 demonstrates the general complementary relationship by paired black lines; the colored lines indicate changes from the general relation due to the two different drought dynamics discussed.

< Figure 2 here >

The two dynamics illustrated in Figure 1—i.e., parallel and complementary ET/E_0 variations—have been observed acting across CONUS. Indeed, Hobbins et al. (2004) revealed that trends in the driving dynamics of E_0 and ET lead to trends in ET that corroborate both complementary and parallel ET/E_0 variations.

Observations of both dynamics can be used to indicate droughts of various types. In flash drought, moisture changes lag behind changes in meteorologic drivers (increasing R_d, for example), causing a transient period during which SM changes slowly, and moisture is still available, while the energy to drive evaporation increases – causing rises in both λET and λE_0 (blue curves in Figure 2a). Mo and Lettenmaier (2015) refer to this type of drought as a "heat wave flash drought" (as distinct from flash droughts driven by rapid Prcp declines) and define it as driven by high T_{air}; we maintain that these droughts may also be driven by the other E_0 drivers (e.g., low q, high R_d or U_2). Whatever the meteorological or radiative forcing, eventually, increased ET decreases the water available for Runoff and depletes SM, leading to both hydrologic and agricultural drought. This time lag in the evaporative signal is short-circuited by use of E_0 anomalies (ΔE_0), which shows the potential changes in the moisture situation before they appear in moisture-related measurements.

In a sustained drought, ET falls in response to limited moisture supply (and follows arrow 1 in Figure 2b). Holding all else equal, Q_n favors increasing H, which heats the dynamic boundary layer and raises its vapor pressure deficit, thereby increasing λE_0 (arrow 2 in Figure 2b). As droughts persist, regional cloudiness decreases and R_d (or Q_n) increases. This dynamic between regional ET and E_0 is the classical understanding of the complementary relationship.

That E_0 should increase in both flash droughts and sustained drought whereas ET responds in opposite directions in these two drought types demonstrates an advantage of EDDI over ET-based drought indices: i.e., ET increases under flash drought initiation, making them insensitive to the onset of such conditions. Central to this study, then, is the concept that, during both flash droughts and sustained droughts, E_0 should demonstrate a surplus relative to its climatological mean. As the drought progresses, this surplus should accumulate, dissipating only when moisture availability or meteorologic and/or radiative forcings at the surface returns to or above their climatological level for some sustained period.

3. Methods and Data

3.1 E_0 from ASCE Standardized Reference ET Equation

For E_0 we use the ASCE Standardized Reference ET (ET_0) formulation (Allen et al. 2005), which provides a widely accepted estimate of E_0. ASCE ET_0 is derived from the Penman-Monteith equation (Monteith 1965), which synthesizes ET_0 as a weighted combination of radiative and advective factors. In particular, ET_0 is function of T_{air}, net radiation R_n at the surface, ground heat flux G, 2-m wind speed U_2, saturated vapor pressure e_{sat} and actual vapor pressure e_a. Reference conditions are assumed to be a well-watered 0.5-m alfalfa crop, completely shading the ground with an albedo of 0.23, though one could also use the 0.12-m grass reference crop.

3.2 Data sources

For the CONUS-wide reanalysis of ET_0, daily inputs are aggregated from the following hourly fields from the North American Land Data Assimilation System phase-2 [NLDAS-2; Mitchell et al. (2004)]: 2-m T_{air} (K), 2-m specific humidity q (kg kg^{-1}), station pressure P_a (Pa), downwelling shortwave radiation R_d (W m^{-2}), and the two orthogonal horizontal 10-m wind vectors U_x and U_y (m sec^{-1}). These data are available from January 1, 1979, to within five days of the present, at a 0.125° spatial resolution (roughly 12 km).

Data sources used for the comparison of EDDI against other basinwide fluxes, states, and indices are as follows: Prcp is extracted from the Parameter Regressions on Independent Slopes Model [PRISM; Daly et al. (1994)]; Runoff data are from USGS data sources for hydrologically undisturbed basins in the Hydroclimatic Data Network [HCDN; Slack and Landwehr (1992)]; SM is available from the Variable Infiltration Capacity [VIC; Liang et al. (1994)] LSM driven by NLDAS-2 forcings; ET is from ALEXI (Anderson et al. 1997). We also use the ALEXI-derived Evaporative Stress Index (ESI) from Anderson et al. (2007), defined as $ESI = ET/E_0$, as another evaporative drought index to which we compare EDDI.

To validate EDDI we use, amongst other measures, the USDM, the *de facto* operational drought-monitoring tool in the United States (US). The USDM is a composite drought indicator, published weekly since January 4, 2000, by the National Drought Mitigation Center (NDMC; http://droughtmonitor.unl.edu/) at the University of Nebraska-Lincoln, the US Department of Agriculture, and the National Oceanic and Atmospheric Administration (NOAA), in an attempt to capture drought intensity, duration, spatial extent and probability of occurrence, while identifying specific drought types (e.g., hydrologic vs. agricultural). The USDM depends heavily on the T_{air}-dependent PDSI, while also surveying a range of other inputs that include ET data (such as ALEXI), and has long been influential across sectors and stakeholder types with respect to drought-response decision-making. Though not completely objective (it incorporates local expert knowledge), it currently serves as the best available benchmark for much drought monitoring research.

3.3 Preliminary Evaporative Demand Drought Index definition

EDDI is formulated as a standardized *Z*-index, which first aggregates a departure of ET_0 from the climatologic mean for a given period of interest, or "aggregation period" *t*, and normalizing it by the climatologic (30-year) standard deviation of daily ET_0 totals aggregated over the same period, as follows:

$$EDDI_t = \frac{ET_{0_t} - \overline{ET_0}_t}{\sigma_{\overline{ET_0}_t}}. \tag{2}$$

in which ET_{0_t} is the daily ET_0 summed over the aggregation period *t* within the year of interest; $\overline{ET_0}_t$ is the mean of ET_{0_t} across N years (here N=30: 1981-2010) of the climatology, and $\sigma_{\overline{ET_0}_t}$ is its standard deviation of ET_{0_t}.

An alternate formulation of EDDI would be to use a distribution fit of the yearly timeseries of $\overline{ET_0}_t$ together with a normal quantile transform to estimate normal deviates that provide the index values. This approach is taken with the Standardized Precipitaiton Index [SPI; McKee et al. (1993)] and Standardized Runoff Index [SRI; Shukla and Wood (2008)], both of which rely on a gamma distribution. The distribution approach is especially suitable for variables with skewed and/or bounded distributions, and would likely be appropriate for the EDDI, especially at shorter timescales. The best choice for the EDDI will depend on the hydroclimate to which EDDI is applied.

A zero EDDI value indicates that no anomaly in ET_0 has accumulated over the aggregation period in the year of interest; negative values indicate wet anomalies; positive EDDI indicates drier than normal conditions, thus drought intensity increases with increasingly positive EDDI. EDDI is multi-scalar in space and time: it may be estimated at a point (or pixel) or by using regional-mean ET_0 over a region; and aggregation periods may vary from as little as one day to a year or more, similar to other multi-scalar drought indices such as the SPI and SRI. These periods would be selected as appropriate to the regional hydroclimatology, sector, user interest, and other criteria (see Section 4.3).

4. Results

The results to follow demonstrate the underlying principles of EDDI and its relevance to drought. Accordingly, the following sub-sections: (1) illustrate the complementary and parallel interactions of ET and E_0 and the E_0 linkage to the water balance; (2) examine how the drivers of E_0 perform under a flash drought and during an in-drought wetting period; (3) demonstrate the multi-scalar, early warning utility of EDDI and offer suggestions on selecting an aggregation window; and (4) demonstrate the consistency of EDDI with other drought indices and monitors.

4.1 Complementary and parallel evaporative dynamics

The drought-related behaviors of E_0, ET, and other hydrologic states, fluxes and E_0-drivers are illustrated using droughts in two river basins – the Russian River basin, which is in northern, coastal California; and the Allegheny River basin, in western Pennsylvania. These basins were chosen in order to represent a variety of hydrologic responses to drought resulting from their differences in hydroclimate, size, topography, and vegetation. The Russian River basin (260 km^2, 100 mi^2) has a Mediterranean climate with a distinct wet, winter season (80% of Prcp falls from November to March period) and a hot, dry summer season. The Allegheny River basin (29,550 km^2, 11,410 mi^2) has a humid continental climate with warm summers and cold winters (with over 1000 mm of snow), and compared to the Russian River basin, a greater annual T_{air} range but much less marked Prcp seasonality (though with a slight summer maximum).

In both basins, we calculate the inter-correlations at the monthly and annual time-scales between basin-averaged ET_0 and water balance variables Prcp, Runoff and SM (Table 1). Monthly data were deseasonalized so as not to artificially inflate the correlations by including intra-annual cycles. Table 1 shows that at both time scales, and in both basins, ET_0 is more strongly linked to the hydrologic cycle than ET. For both basins, Prcp, Runoff and SM are, unsurprisingly, strongly inter-related at the annual scale, while at the monthly scale, these relationships vary between basins. In the Russian River basin, the ET_0-SM correlation is higher (R^2 = 83%) than for any other variable pairs, and it is also one of the strongest correlations at the monthly timescale (34%). SM does not correlate at all with monthly ET. In fact, ET correlates weakly with all other water balance components at the monthly time scale (its highest correlation is with ET_0 at 9.5%; all others are below 5%). Across the larger Allegheny River basin, water balance correlations involving ET and ET_0 are both relatively weak, again with the exception of annual ET_0-SM (48%), although even at the monthly timescale SM is more strongly correlated to ET_0 (25%) than to ET (1.4%).

< Table 1 here >

Figure 3 portrays the two ET-ET_0 regimes previously described—parallel and complementary—and shows the extent to which complementarity holds in the two basins. In general, the relationship holds well in the Russian River basin (CA), but poorly in the Allegheny River basin (PA). ET and ET_0 are shown as a function of water availability (represented by monthly Prcp plus mean monthly SM). Though not non-dimensional [which is preferred by Kahler and Brutsaert (2006)], the complementarity patterns are usefully expressed.

For the Russian River (Figure 3a-b), in both wet and dry seasons, ET_0 declines with increasing Prcp—indicating the effects of extra cloudiness, lower irradiance and sensible heating of the dynamic boundary layer from the surface, in favor of higher latent heat flux (λET). The complementarity is particularly strong during the drier, moisture-limited summer months, when ET becomes water limited and declines while ET_0 increases with energy availability. In contrast, during the high-Prcp winter periods (January to May), water is available for ET (Figure 3a), ET is energy-limited and increases in line with increasing energy availability (and hence with ET_0). Thus, both parallel (November to March) and complementary (May to September) ET-ET_0 interactions occur within the year. At annual time scales (not shown) these moisture and energy differences average out and the overall ET-ET_0 complementarity becomes more evident.

Across the Allegheny River basin (Figure 3c-d), on the other hand, ET-ET_0 complementarity is not evident in either wet or dry periods. This may be due to the fact that the greater water storage can mediate the meteorological and radiative variations that drive ET_0 variability, even at seasonal time scales, leaving moisture for sustained ET long after ET_0 conditions might indicate otherwise, and leading to a weaker coupling between the land surface and the atmosphere at shorter time scales. The effects of this regional variation in coupling strength on the performance of EDDI are examined in more detail in the companion paper (McEvoy et al. - this issue).

< Figure 3 here >

In **Figure 4**, which demonstrates as time series the 14-year development of various water balance components for the Russian River basin, data are accumulated (or averaged, for SM) across a 12-month moving window that steps monthly. The parallel responses of SM and Runoff to Prcp are immediately clear. To a lesser degree, ET also tracks Prcp well, increasing during the highest Prcp periods of 2002-2007 and 2010-2012. However, ET does not only vary in response to the availability of water (from Prcp and SM) but also of energy (as reflected in ET_0). During water-limited periods when there is enough energy available to evaporate moisture, ET and ET_0 vary in a complementary fashion (Figure 4 periods 1, 3 and 5). During energy-limited periods when there is enough moisture to evaporate at prevailing energy conditions, ET and ET_0 vary in a parallel fashion (Figure 4 periods 2, 4 and 6).

< Figure 4 here >

4.2 Decomposing drought evaporative dynamics

It is instructive to explore how variations of components of E_0—T_{air}, q, R_d, and U_{10}—relate to E_0 and EDDI under varying conditions of drought, and to decompose and attribute the evaporative signature of drought to its meteorologic drivers. Variations in our E_0 metric accumulate as a function of both the anomalies in these driving variables and the sensitivities of E_0 to them, as follows:

$$\Delta E_0 = \frac{\partial E_0}{\partial T}\Delta T + \frac{\partial E_0}{\partial R_d}\Delta R_d + \frac{\partial E_0}{\partial q}\Delta q + \frac{\partial E_0}{\partial U_{10}}\Delta U_{10}. \tag{3}$$

Each term on the RHS represents the contribution to the surplus in E_0 by each driving variable (for analytical solutions to the derivatives and a CONUS-wide assessment, see Hobbins 2015). Which terms dominate variations in E_0 has been shown across CONUS and seasons for synthetic pan evaporation in Hobbins et al. (2012) and in Hobbins (2015) for ASCE ET_0. Clearly these variations combine to determine the variability of the evaporative drivers and responses of drought. These terms give insight into the meteorological factors contributing to the flash drought and into whether the ET_0 analysis (and EDDI) provides advance warning. In Figure 5a, for example, the E_0 signal of a period of flash drought is related to its driving variables using Eqn. (3) at a two-week aggregation period for the calendar year 2012 to summer 2013 in the Current River basin in southern Missouri. The drought period is portrayed by the USDM (Figure 5b) starting in May but rapidly deepening through June to peak intensity in August, before abating. The top panel of Figure 5a tracks the two-week anomalies (ΔET_0) and the contributions to ΔET_0 of each of the four drivers ($\Delta T_{air}. \partial E_0/\partial T_{air}$ for T_{air}, similarly for q, R_d, and U_2), in mm depths accumulated across a two-week period stepping daily. In the lower five panels, daily ET_0 and its four drivers throughout the year are also plotted with their 30-year (1981-2010) daily means for comparison. T_{air} and q make the largest contributions to ΔET_0 from their own anomalies: with the majority of T_{air}'s contributions to ΔET_0 being positive, and q's being negative until late-May and positive thereafter. The contribution from high U_2 is small by comparison (though always positive) until early June, when it climbs to 10-20 mm until late-October, coinciding with the intensification of drought conditions. This is confirmed by the daily U_2 trace, which is generally above normal from June to September. Although R_d is often above normal, ET_0's minimal sensitivity to R_d in this region [see Hobbins (2015)] results in it making little contribution to ΔET_0 across the year.

< Figure 5 here >

We note that the contribution from the above-normal T_{air} early in the year is largely mediated by above-normal q, leaving ΔET_0 near zero after February. In March and April both T_{air} and q spike well above their normal, with q making a negative contribution of almost -60 mm to ΔET_0 but T_{air} making a positive contribution of 60 mm and combining with U_2 contributions to steadily increase ΔET_0 (and so increase EDDI). In late-May, the anomaly in q switches signs and combines with the still positive T_{air} anomaly, leading ΔET_0 to climb rapidy, to a two-week surplus in early July of 80 mm. This is recorded by the USDM as a "flash drought" or a sudden increase in USDM drought category across the basin. The event was to some extent foreshadowed in the previous months by a high EDDI, leading up to an EDDI peak at nearly 10 (i.e., ~10 stdevs above the mean); as shown in Figure 5b, the short-term EDDI peaks approximately one month before the USDM reported a maximum drought intensity (D4 drought category).

The rapid return to near-normal conditions for ET_0 in late July is driven by a rapid return to near-normal T_{air} and q combined with a sudden negative anomaly in U_2. However, these conditions last for only a few weeks before the drivers return to severe drought conditions and the ET_0 surplus peaks again, and then extends throughout the rest of the summer into the fall. In late-October, all drivers have returned to near-normal conditions and, as metered by short-term EDDI, the drought is significantly ameliorated and eliminated early in the following year. Considering these results, it is possible that the ET_0 and two-week EDDI presaged drought in early March; yet is is unclear whether the high EDDI conditions in the spring were a necessary table-setting for the descent into drought later. Certainly variation in the drivers of EDDI just before and during the event were consistent with drought, and the physical framework for decomposing E_0 provides insight into proximate factors influencing the drought. For more detail on this event and EDDI's ability to provide early warning, see the companion paper (Figures 6 and 7; McEvoy et al. - this issue).

A contrasting case is provided by the E_0 behavior during a significant within-drought wetting event in the Russian River basin in Sonoma County. From November 28 to December 21, the most intense period of the 2011-current California drought, an atmospheric river (AR) made landfall across Northern California. Three pulses of rain were recorded at Santa Rosa Airport (station KSTS): 107 mm (4.23 in) from 28 November to 5 December; 162 mm (6.39 in) during 10-12 December; and 127 mm (5.01 in) from 15-20 December. As shown in Figure 6*,* the wetting signal is evident in short-term (1-week) EDDI and in ET_0 and its contributing inputs.

< Figure 6 here >

The three Prcp pulses are more clearly resolvable as individual ET_0 declines in its daily timeseries (third panel of Figure 6a) than as ΔET_0 declines (top panel) due to the 1-week memory mediating such immediate responses in the latter. There is a significant decline in EDDI over the entire period as the wetting event progresses, forced primarily by a positive q anomaly driving ET_0 downward for all but the last day of the period. This negative q-forcing counteracts the combined effects of the period-long positive T_{air} and R_d anomalies after December 5 and elevated U_2 from December 3-18 typical of AR landfall events, which all act to raise ET_0. The contrasting effects of drivers acting at different periods across the event combined to generate a noisy ET_0 signal that was nonetheless ultimately downward. The maps reflect the very different time frames at which the USDM and 1-week EDDI operate. The 1-week EDDI oscillates rapidly between dry and wetter conditions as the pulses of moisture impact the region, whereas the USDM varies little in response, only decreasing by a single drought category in northern CA alone. As shown by Figure 6b, the short-range integration EDDI reflects mainly the transient weather-scale signals; however EDDI at this time scale remains unsuitable for drought characterization, which for purposes of long-term impacts (such as low reservoirs) would be better served by simultaneously estimating EDDI at a monthly or longer scale. The multi-scalar property of EDDI is addressed in Section 4.3.

4.3 EDDI as a multi-scalar, leading indicator

Following the SPI and other drought indices, EDDI is formulated as a multi-scalar metric from which specific time-aggregated versions can be selected (e.g., from 1 week to 12 months or longer). Depending on location, certain aggregations can provide a leading indication of drought development. We illustrate this behavior using two basins—the Current River at Doniphan, MO (USGS 07068050) and the Colorado River near Cisco, UT (USGS 09180500; hereafter the "Upper Colorado River basin")—that differ in size, land cover, topography and hydroclimate. The Current River basin is a primarily forested (78% by area) basin of only 5,224 km^2 located in the agricultural Midwest, with a mean elevation of 300 m a.s.l. (Slack and Landwehr 1992) and a rainfall-dominated hydroclimate. The Upper Colorado River drainage is much larger at 61,770 km^2 and is far more spatially heterogeneous—typified by the high mountain ranges and sparse forests of the central Rocky Mountains, intervening rangeland, and occasional irrigated valleys—and has a snowmelt-dominated hydroclimate.

In each of the two basins, the time evolution of different scalar versions of EDDI are compared to the USDM analysis over a period of 15 years (Figures 7 and 8, for Current and Upper Colorado River basins, respectively). By design, the shorter-range EDDIs fluctuate rapidly while the longer range EDDIs change gradually, and the spread of the various EDDI traces arises from the drying and wetting EDDI responses on the different time scales. The figures illustrate that the fast-responding EDDIs offer the most potential for depicting an impending change in drought condition, but are unreliable for characterizing the severity of an established drought. Shorter period EDDI*s* may be particularly useful in smaller basins that respond rapidly to intense, high-frequency events, such as the Current River (Figure 7). Here, both the short- and long-time scale EDDI give early warning (with respect to the USDM) of the two most significant droughts—during 2011 and the flash drought in 2012 (see Figure 5 and Section 4.2 for more on this drought). For example, the longer-term EDDI traces increase approximately six months in advance of the USDM's 2011 drought. Further, observe that while the USDM distinguishes between these two droughts, both long- and short-term EDDI remain elevated between them, indicating that, despite the USDM reporting that the 2011 drought has ended, the extra information contained in the EDDI index shows that at no time scales have evaporative conditions returned to normal, setting the stage for a rapid re-emergence of drought in 2012.

< Figure 7 and Figure 8 here >

Longer time scale EDDI*s* may more usefully capture the slower response of larger basins or those with significant snowmelt-lagged hydroclimates, such as the Upper Colorado River basin

(Figure 8). Here the short-range EDDIs appear to have little relationship to drought variations, indicating a mis-match between these time scales and the basin's spatial scale and/or snowmelt-dominated hydroclimatology. On the other hand, the longer timescale EDDIs appear to offer early warning information: not only do many of the monthly EDDIs start increasing well in advance of the USDM registering drought onset (see 2001, 2007, 2008, 2010, and 2015), but they remain elevated in inter-drought periods as indicated by the USDM (see 2011) and, for ongoing droughts (again indicating the extra information contained in the EDDI index that is as yet missing from the USDM), also show both increasing severity (see 2002, 2005, and 2012) and amelioration (see 2013 to 2014).

Overall, the multi-weekly and monthly-to-seasonal EDDI are likely be of the most use, but the best aggregation period to provide leading or ongoing information about drought depends on the hydroclimatology of the region of interest, and on users' sector-specific needs. The correlation analysis of Figure 6 provides a useful diagnostic approach for selecting an optimal window size. The correlation surface shows the association between EDDI and USDM for aggregation period-lengths varying from 1-12 weeks and 1-12 months, for various lag and lead times between the two time series, for four hydroclimatically different basins. To the right of the vertical dashed line at 0-lag, EDDI leads USDM.

< Figure 9 here >

The correlation surfaces differ between basins due to their hydroclimates. For example, in the Upper Colorado River basin, the 10- to 12-month optimal aggregation period yields a lead-time over the USDM of up to four months, while there is little association between EDDI and USDM at the shorter one- to three-weekly aggregation periods. The long lead time and aggregation periods is related to the significant lagged influence of snowpack on river flow anomalies. Dry climate anomalies in the snow accumulation period are reflected in the EDDI signal but may be only be reflected in the USDM signal in the following growing/irrigation season. In contrast, in the Apalachicola River basin, which has little to no snow, the greatest information content in short-term EDDI is for a three-week aggregation period, which leads the USDM signal by 12 weeks.

A distinct characteristic of the correlation surfaces is that, at longer aggregation periods, the USDM appears to lead EDDI—observe the "leaning" of the correlation space towards the left at longer EDDI aggregation periods. This is most likely due to the nature of the USDM, which is a blend of non-physical inputs (such as expert local knowledge) and physical inputs at a variety of time-scales. Many of these physical inputs will be at shorter time scales than long-term EDDI, and will therefore be more reactive to short-term transient meteorological and/or radiative forcings than the EDDI, which reacts more slowly due to its long memory. This hypothesis bears further investigation but, overall, the shape of the correlation surfaces do appear to favor EDDI as a leading indicator of the USDM at EDDI aggregations of period-lengths below a threshold that depends on the basin.

4.4 Consistency of EDDI with other drought measures

To demonstrate the consistency of EDDI with other drought metrics, Figure 10 compares the 3-month EDDI (Figure 10b) with the USDM (Figure 10a), the VIC-modeled soil moisture percentiles (Figure 10c) from the Surface Water Monitor (Wood 2008), and the ESI (Figure 10d) from ALEXI (Anderson et al. 2007) for the same date—August 1, 2002, during a significant drought event over much of western CONUS. All four drought measures indicate drought via the drier than normal conditions across most of the western states (the exception being much of WA), centered on the Four Corners region and the Central High Plains; also, to a lesser degree, in the mid-Atlantic states. Examination of EDDI at other time scales (not shown) indicates that at this date, the drought on the East Coast is becoming less intense, while that in the Southwest and Central High Plains is at peak intensity.

< Figure 10 here >

There are nonetheless differences between all measures shown. EDDI shows two lobes of >95%ile drought (equivalent to the USDM D3 and D4 drought categories) in the Central High Plains of eastern CO and WY, western KS, and NE, and one to the southwest in AZ, drought is observed at lesser intensities across almost the entire western US. The eastern seaboard drought is centered on northern NC, VA, MD, DE, and southern PA and NJ, but extends at lesser intensities south into SC and north into NY and New England. The USDM agrees with the configuration of EDDI*'s* western drought but shows the most intense region of the eastern drought further south down the Atlantic Seaboard, from GA to MD. The SWM SM map agrees spatially with the EDDI map although it indicates > 95%ile drought over a larger extent, while it understates the severity of the eastern seaboard drought relative to EDDI and places its centroid further south down the coast, in line with the USDM. The ESI matches EDDI the most closely, indicating almost identical extent and severity of the eastern seaboard drought, and the Central High Plains lobe of the western drought. However the southwestern lobe of the western drought is shown as less severe in ESI than in EDDI, and, significantly, severe drought extends north and east into the Northern High Plains of SD and ND and into MN. Notably, the two evaporatively based drought indices indicate the greatest agreements as to location and severity of drought.

5. Discussion and conclusions

This paper represents the exploratory study into the physical basis and utility of a drought index based on evaporative demand alone—the Evaporative Demand Drought Index (EDDI). A companion paper (McEvoy et al. - this issue) verifies the performance of EDDI with respect to other drought metrics across CONUS. The key rationale for EDDI is that E_0 reflects drying (and wetting) anomalies through feedbacks with ET and other water balance components that implicitly encode moisture availability. We describe ET-E_0 inter-relations under various drought types and observe both complementary and parallel ET-E_0 (hence EDDI) interactions operating in several basin case studies. Having established the E_0-drought connection, we decompose the evaporative drivers of drought dynamics for both a flash drought and a within-drought wetting event. We illustrate the multi-scale properties of EDDI and its potential to serve as a leading indicator for drought condition changes. Finally, we use an example to show that the EDDI depiction of sustained drought is generally consistent with other drought-monitoring metrics.

Our main findings are as follows:

- E_0 is more highly correlated with the main hydrologic components of the water balance than is ET, but complementary and parallel ET-E_0 dynamics yield a robust signal in E_0 that responds to both dry and wet anomalies across time scales. While the overall ET-ET_0 relationship is at first glance weak, this is due to their inter-relationship being both positive (parallel interactions) and negative (complementary interactions). ET_0's high correlation with SM underlines both its role as a predictor of meteorologic variability and moisture availability within the agricultural sector and its potential as a monitor of agricultural drought.
- The EDDI that converts E_0 into a drought index is both easy to compute and, depending on the forcing variables' origin, available in near-real time. A significant caveat is that a physically based E_0 measure must be used—not a T_{air}-based parameterization.

- EDDI detects both flash and sustained droughts in a manner that is consistent with the USDM and other SM- and ET-based drought metrics in both pattern and intensity. The combination of E_0's rise in response to both fast-developing and sustained droughts often weeks to months prior to the USDM and the driving variables' relatively low latency—about five days for our NLDAS-based E_0—suggest EDDI's utility in real-time drought monitoring and as a robust drought leading indicator.
- EDDI's multi-scalar properties permit different drought-monitoring functionalities as the signals of various drying dynamics are evident at different time scales: short-term EDDI may serve as a drought early warning signal, especially in agricultural areas; long-term EDDI may be useful for water-limited hydrologic drought monitoring. Operational time frames will vary with hydroclimate, scale, and sector, but their optimization is straightforward.

This exploratory paper suggests many directions for future research. Beyond EDDI itself, improvements to the USDM to its treatment of evaporation—currently limited to ET estimation from LSMs, and physics-poor implementations hidden inside other drought tools—could accrue by inclusion of the NLDAS-forced E_0 reanalysis (the ET_0 underpinning EDDI) as a driver of LSMs and drought indices. Indeed, on time scales pertaining to both ongoing and flash droughts, using a physically based observed E_0 driver that is spatially distributed, well-calibrated, physically representative, and available on a daily basis with limited latency will enhance characterization of the evaporative dynamics of ongoing drought, and the resulting EDDI can provide a perspective that is as yet missing. Potential drought onsets could be identified via high-frequency E_0 surpluses using a small aggregation period filter and then verified using a longer aggregation period filter. Non-standard uses of EDDI are already underway: it is currently in experimental use by USFS Southern Research Station in their seasonal forecasts of large fires on US lands and their suppression costs (Ham et al. 2014). Forecasts of E_0 itself—currently produced at the daily and weekly time scales by the National Weather Service (Snell et al. 2013) and forthcoming at the seasonal time scale—suggest the possibility of drought forecasting from the evaporative perspective. Overall, explicating the role of E_0 in drought occurrence will deepen our understanding of water and energy cycle phenomena, thereby improving operational water management, drought monitoring and prediction, and decision-making in water-dependent sectors.

Acknowledgments

The NLDAS data were acquired as part of the mission of NASA's Earth Science Division and archived and distributed by the Goddard Earth Sciences (GES) Data and Information Services Center (DISC). The lead author acknowledges support from by Inter-Agency Agreement AID-FFP-P-10-00002/006 between USAID and NOAA for support to the Famine Early Warning Systems Network.

References

Allen, R.G., I.A. Walter, R. Elliott, T. Howell, D. Itenfisu, and M. Jensen, 2005: The ASCE standardized reference evapotranspiration equation. Report 0-7844-0805-X, 59 pp. [Available online at http://www.kimberly.uidaho.edu/water/asceewri/ascestzdetmain2005.pdf.]

Anderson, M.C., J.M. Norman, G.R. Diak, W.P. Kustas, and J.R. Mecikalski, 1997: A two-source time-integrated model for estimating surface fluxes using thermal infrared remote sensing. *Remote Sens. Environ.*, **60**, 195–216.

Anderson, M.C., J.M. Norman, J.R. Mecikalski, J.A. Otkin, and W.P. Kustas, 2007: A climatological study of evapotranspiration and moisture stress across the continental United States based on thermal remote sensing: 2. Surface moisture climatology, *J. Geophys. Res.*, **112**, D11112, doi:10.1029/2006JD007507.

Bouchet, R.J., 1963: Évapotranspiration réelle et potentielle, signification climatique. *Proc. International Association Scientific Hydrology Symp., Publ. No. 62*, Berkeley, CA, International Association Scientific Hydrology, 134–142.

Dai, A., K.E. Trenberth, and T. Qian, 2004: A global dataset of Palmer Drought Severity Index for 1870– 2002: Relationship with soil moisture and effects of surface warming. *J. Hydrometeor.*, **5**, 117–130.

Daly, C., R.P. Neilson, and D.L. Phillips, 1994: A statistical-topographic model for mapping climatological precipitation over mountainous terrain. *J. Appl. Meteorol.*, **33(2)**, 140–158.

Ham, C., M.T. Hobbins, K.L. Abt, and J.P. Prestemon, 2014: Using the Evaporative Demand Drought Index and the Palmer Drought Severity Index to forecast the number of large wildland fires on federal lands, *Large Wildland Fires Conference*, Missoula, MT, Association for Fire Ecology and the International Association of Wildland Fire. [Available online at http://largefireconference.org/wp-content/uploads/2013/06/Oral-Presentation-Abstracts-V4.pdf.]

Hargreaves, G.H., and Z.A. Samani, 1985: Reference crop evapotranspiration from temperature, *Appl. Eng.Agric.*, **1**, 96–99.

Hobbins, M.T., J.A. Ramírez, and T.C. Brown, 2004: Trends in pan evaporation and actual evaporation across the conterminous U.S.: Paradoxical or complementary? *Geophys. Res. Lett.*, **31(13)**, L13503, doi: 10.1029/2004GL0198426.

Hobbins, M.T., A. Dai, M.L. Roderick, and G.D. Farquhar, 2008: Revisiting the parameterization of potential evaporation as a driver of long-term water balance trends. *Geophys. Res. Lett.*, **35**, L12403, doi: 10.1029/2008GL033840.

Hobbins, M.T., A.W. Wood, D. Streubel, and K. Werner, 2012: What drives the variability of evaporative demand across the conterminous United States? *J. Hydrometeor.*, **13**, 1195–1214, doi: 10.1175/JHM-D-11-0101.1.

Hobbins, M.T., 2015: The variability of ASCE Standardized Reference Evapotranspiration: a rigorous, CONUS-wide decomposition and attribution. *Trans. ASABE* (accepted).

Kahler, D.M., and W. Brutsaert, 2006: Complementary relationship between daily evaporation in the environment and pan evaporation. *Water Resour. Res.*, **42**, W05413, doi:10.1029/2005WR004541.

McEvoy, D.J., J.L. Huntington, M.T. Hobbins, A. Wood, C. Morton, and J. Verdin, 2015: The Evaporative Demand Drought Index: Part II – CONUS-wide assessment against common drought indicators. *J. Hydrometeor.* (this issue).

McKee, T.B., N.J. Doesken, and J. Kleist, 1993: The relationship of drought frequency and duration to time scales. *Preprints, Eighth Conf. on Applied Climatology*, Anaheim, CA, Amer. Meteor. Soc., 179–184. [Available online at http://ccc.atmos.colostate.edu/relationshipofdroughtfrequency.pdf.]

Mitchell, K.E., and Coauthors, 2004: The multi-institution North American Land Data Assimilation System (NLDAS): Utilizing multiple GCIP products and partners in a continental distributed hydrological modeling system, *J. Geophys. Res.*, **109**, D07S90, doi:10.1029/2003JD003823.

Mo, K.C., and D.P. Lettenmaier (2015), Heat wave flash droughts in decline. *Geophys. Res. Lett.*, **42**, 2823–2829, doi:10.1002/2015GL064018.

Monteith, J.L., 1965: Evaporation and environment. *Symp. Soc. Exp. Biol.*, **XIX**, 205–234.

Mu, Q., M. Zhao, J.S. Kimball, N.G. McDowell, and S.W. Running, 2013: A remotely sensed global terrestrial drought severity index. *Bull. Amer. Meteor. Soc.*, **94(1)**, 83–98, doi:10.1175/BAMS-D-11-00213.1.

Narasimhan, B., and R. Srinivasan, 2005: Development and evaluation of Soil Moisture Deficit Index (SMDI) and Evapotranspiration Deficit Index (ETDI) for agricultural drought monitoring. *Agricultural and Forest Meteorology*, **133**, 69–88, doi:10.1016/j.agrformet.2005.07.012

Palmer, W.C., 1965: Meteorological drought. Research Paper 45, 58 pp. [Available online at http://www.ncdc.noaa.gov/temp-and-precip/drought/docs/palmer.pdf.]

Pettijohn, J.C., and G.D. Salvucci, 2009: A new two-dimensional physical basis for the complementary relation between terrestrial and pan evaporation. *J. Hydrometeor.*, **10**, 565–574, doi:10.1175/2008JHM1026.1.

Roderick, M.L., L.D. Rotstayn, G.D. Farquhar, and M.T. Hobbins, 2007: On the attribution of changing pan evaporation. *Geophys. Res. Lett.*, **34**, L17403, doi:10.1029/2007GL031166.

Roderick, M.L., M.T. Hobbins, and G.D. Farquhar, 2009: Pan evaporation trends and the terrestrial water balance. I. Principles and observations. *Geography Compass*, **3/2**, 746–760, doi:10.1111/j.1749-8198.2008.00213.x.

Sheffield, J., E.F. Wood, and M.L. Roderick, 2012: Little change in global drought over the past 60 years. *Nature*, **491**, 435–438, 15 November, doi:10.1038/nature11575.

Shukla, S., M. Safeeq, A. AghaKouchak, K. Guan, and C. Funk, 2015: Temperature impacts on the water year 2014 drought in California. *Geophys. Res. Lett.* (in press).

Shukla, S. and A.W. Wood, 2008: Use of a standardized runoff index for characterizing hydrologic drought, *Geophys. Res. Lett.*, **35**, L02405, doi:10.1029/2007GL032487.

Slack, J.R., and J.M. Landwher, 1992: Hydro-climatic Data Network (HCDN): A U.S. Geological Survey streamflow data set for the United States for the study of climate variations, 1974-1988. U.S. Geological Survey Open-File Report 92-129, 193 pp. [Available online at http://pubs.usgs.gov/of/1992/ofr92-129/.]

Snell, H.D., C.K. Palmer, P. Krone-Davis, F.S. Melton, and M.T. Hobbins, 2013: National Weather Service Forecast Reference Evapotranspiration. Abstracts, *2013 Fall Meeting*, San Francisco, CA, Abstract H21A-1012, American Geophysical Union. [Available online at http://abstractsearch.agu.org/meetings/2013/FM/H21A-1012.html.]

Szilagyi, J., 2007: On the inherent asymmetric nature of the complementary relationship of evaporation. *Geophys. Res. Lett.*, **34**, L02405, doi:10.1029/2006GL028708.

Thornthwaite, C.W., 1948: An approach toward a rational classification of climate. *Geogr. Rev.*, **38**, 55–94.

Vicente-Serrano, S.M. , S. Beguería, and J.I. López-Moreno, 2010: A multiscalar drought index sensitive to global warming: The standardized precipitation evapotranspiration index. *J. Climate*, **23(7)**, 1696–1718, doi:10.1175/2009JCLI2909.1.

Wood, A.W., 2008: The University of Washington Surface Water Monitor: An experimental platform for national hydrologic assessment and prediction. *Proc., 22nd Conf. on Hydrology*, New Orleans, LA, Amer. Meteor. Soc., 13 pp. [Available online at http://ams.confex.com/ams/pdfpapers/134844.pdf.]

Xia, Y., M.B. Ek, C.D. Peters-Lidard, D. Mocko, M. Svoboda, J. Sheffield, and E.F. Wood, 2014: Application of USDM statistics in NLDAS-2: Optimal blended NLDAS drought index over the continental United States. *J. Geophys. Res.-Atmospheres*, **119**, doi:10.1002/2013JD020994.

Yin, D., M.L. Roderick, G. Leech, F. Sun, and Y. Huang, 2015: The contribution of reduction in evaporative cooling to higher surface air temperatures during drought. *Geophys. Res. Lett.* (in press).

Table 1: Coefficients of determination (R^2) for relationships between basin-averaged one-month (italics) and 12-month (bold) simulated water-balance components for **(top)** the Russian River basin, and **(bottom)** the Allegheny River basin, from January, 2000, to December, 2013.

Russian River basin

	ET_0	ET	Prcp	Runoff	SM
ET_0	1	**0.408**	**0.361**	**0.487**	**0.826**
ET	*0.095*	1	**0.030**	**0.028**	**0.380**
Prcp	*0.172*	*0.014*	1	**0.626**	**0.635**
Runoff	*0.162*	*0.020*	*0.619*	1	**0.652**
SM	*0.339*	*0.041*	*0.241*	*0.489*	1

Allegheny River basin

	ET_0	ET	Prcp	Runoff	SM
ET_0	1	**0.115**	**0.118**	**0.273**	**0.484**
ET	*0.059*	1	**0.000**	**0.018**	**0.009**
Prcp	*0.072*	*0.005*	1	**0.860**	**0.507**
Runoff	*0.064*	*0.000*	*0.464*	1	**0.572**
SM	*0.246*	*0.014*	*0.247*	*0.398*	1

List of figures:

Figure 1: Location of the five basins used in this study, including NLDAS elevation (m) above mean sea level.

Figure 2: Idealized responses of ET and E_0 to varying moisture and energy conditions: **(a)** varying in parallel; and **(b)** varying in a complementary relationship.

Figure 3: The ET-ET_0 relationship in the Russian River basin (CA) during **(a)** the cool, wet October-March period, and **(b)** the warm, dry April-September period, and in the Allegheny River basin (PA) during **(c)** the cool October-March period, and **(d)** the warm April-September period.

Figure 4: Linkages between areally averaged simulated water balance components. Time-series of basinwide variations in ET_0, ET, Runoff, Prcp, and SM for the Russian River basin (CA) from January, 2010, to December, 2013, with each series mean shown as a horizontal line. Units for ET_0, ET, Prcp, and Runoff are mm year^{-1}; units for SM are mm. Numbered shaded periods denote periods discussed in the text.

Figure 5: Example of time variations of ΔET_0 and its drivers under a flash drought during the spring and summer of 2012, in the Current River basin (MO). In **(a)** the top panel shows 2-week time series of ΔET_0 (mm) and each driver's contributions to ΔET_0 (mm); lower panels show daily time series of ET_0 (mm d^{-1}), T_{air} (^{o}C), q (kg kg^{-1}), R_d (W m^{-2}), and U_2 (m s^{-1}), respectively, with daily climatological (1981-2010) mean values in black. In **(b)** the time series of drought monitors across the basin are shown for a two-year period 2012-2013 including the flash drought: 1- to 12-weekly EDDI in the top panel; 1- to 12-monthly EDDI in the middle panel; weekly USDM plotted as percentage of basin in each USDM drought category in the bottom panel (the full time series is shown in Figure 7).

Figure 6: Example of time variations of ΔET_0 and its drivers under an intra-drought wetting interval (the landfall of an atmospheric river) from November 28 to December 21, 2014, in the Russian River basin (CA). In **(a)** the top panel shows 1-week time series of ΔET_0 (mm) and each driver's contributions to ΔET_0 (mm); lower panels show, in descending order, daily time series of Prcp (mm, recorded at the Santa Rosa, CA, weather station 047965, located within the basin), ET_0 (mm), T_{air} (^oC), q (kg kg^{-1}), R_d (W m^{-2}), and U_2 (m s^{-1}), with daily climatological (1981-2010) mean values in black. In **(b)** the progression of drought monitors is mapped across CA and NV for the same period: USDM on left; 1-week EDDI on right.

Figure 7: Basinwide time variations of multi-weekly and multi-monthly EDDI and USDM for the entire USDM period (from January 4, 2000 to the present) across the Current River basin (MO). **(Top)** is for one- to 12-monthly EDDI; **(middle)** is for the one- to 12-weekly EDDI; **(bottom)** is for weekly USDM.

Figure 8: Basinwide time variations of multi-weekly and multi-monthly EDDI and USDM for the entire USDM period (from January 4, 2000 to the present) across the Upper Colorado River basin. **(Top)** is for one- to 12-monthly EDDI; **(middle)** is for the one- to 12-weekly EDDI; **(bottom)** is for weekly USDM.

Figure 9: Correlations between river basin spatial means of USDM and EDDI. EDDI varies from 1- to 3-week and 1- to 12-month aggregation periods shown on the ordinate axes, with lead (lag) times between USDM and EDDI of up to +/- 12 weeks and months (for weekly and monthly EDDI, respectively), shown on the abscissae. Correlations are indicated by color: red positive; blue negative.

Figure 10: Comparing representations of drought conditions of mid-summer, 2002: **(a)** the USDM on July 30, 2002; **(b)** the three-month EDDI on July 31, 2002; **(c)** percentiles of VIC-

modeled soil moisture (SM) from the University of Washington Surface Water Monitor (Wood 2008) on July 31, 2002; and **(d)** 12-week ESI (Anderson et al. 2007) on July 29, 2002.

Figure 1

Click here to download Rendered Figure: EDDI_Part_I_Hobbins_et_al - figure 1.pdf

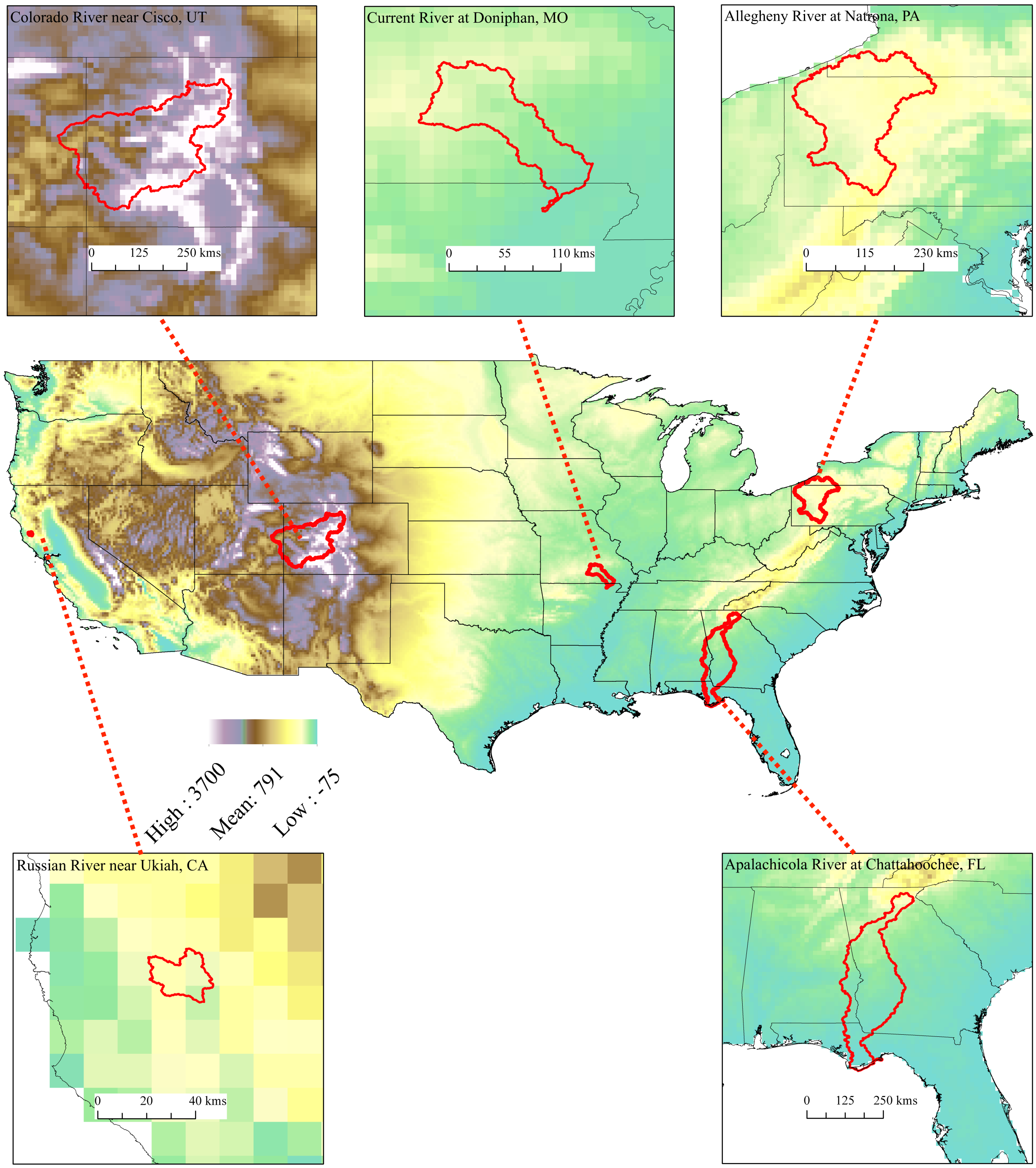

Figure 1: Location of the five basins used in this study, including NLDAS elevation (m) above mean sea level.

Figure 2
Click here to download Rendered Figure: EDDI_Part_I_Hobbins_et_al - figure 2.pdf

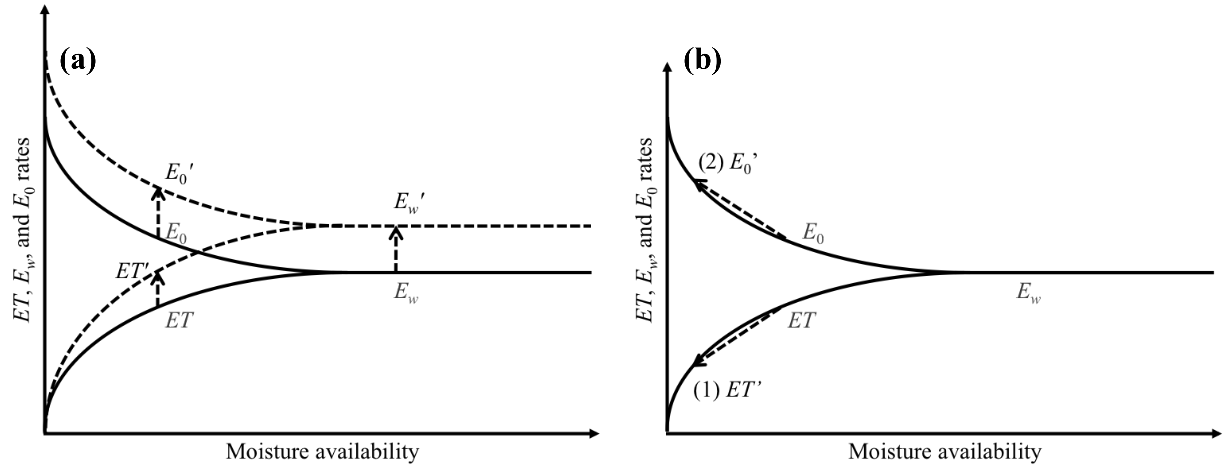

Figure 2: Idealized responses of ET and E_0 to varying moisture and energy conditions: **(a)** varying in parallel; and **(b)** varying in a complementary relationship.

Figure 3
Click here to download Rendered Figure: EDDI_Part_I_Hobbins_et_al - figure 3.pdf

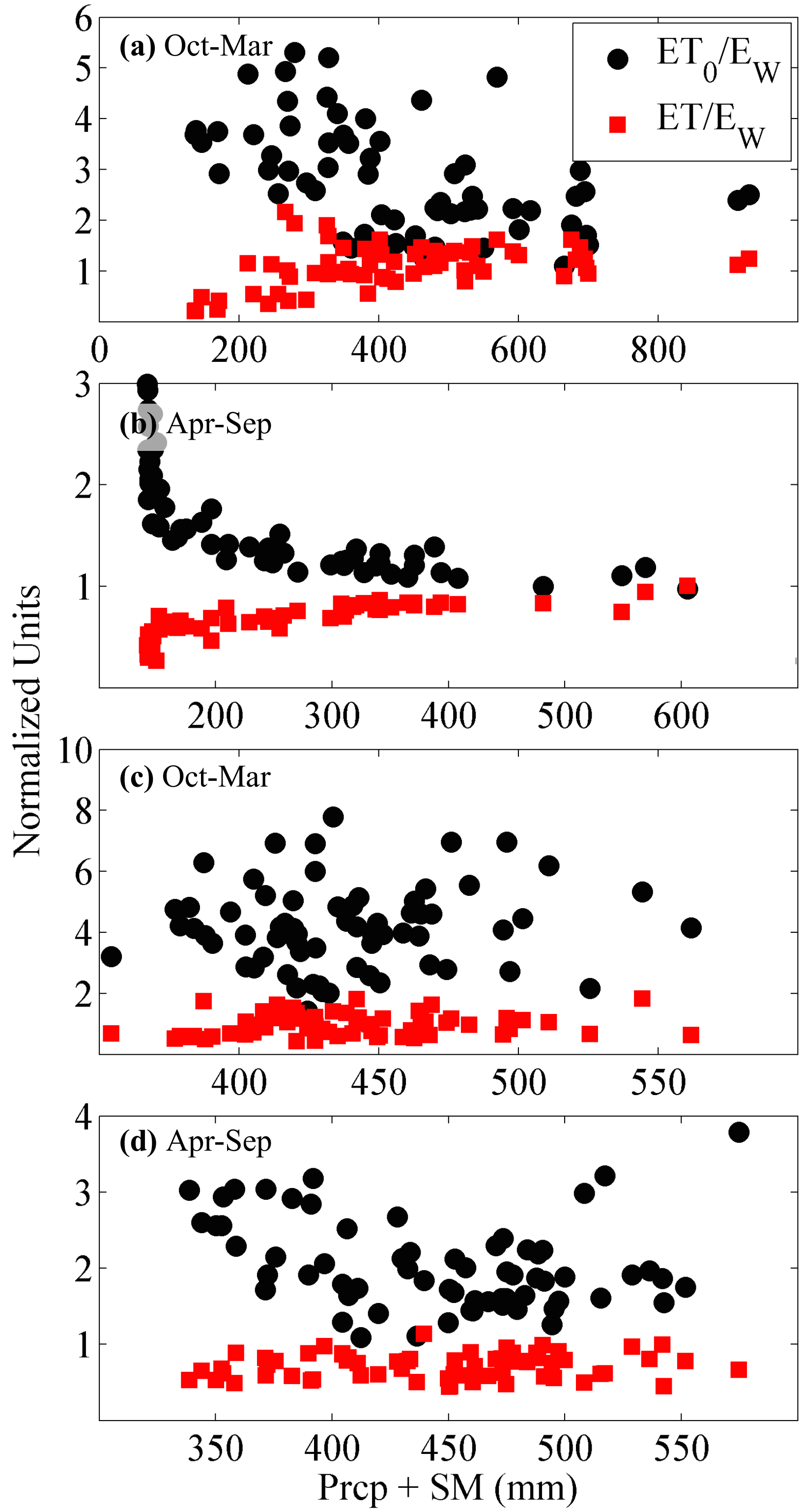

Figure 3: The ET-ET$_0$ relationship in the Russian River basin (CA) during **(a)** the cool, wet October-March period, and **(b)** the warm, dry April-September period, and in the Allegheny River basin (PA) during **(c)** the cool October-March period, and **(d)** the warm April-September period.

Figure 4
Click here to download Rendered Figure: EDDI_Part_I_Hobbins_et_al - figure 4.pdf

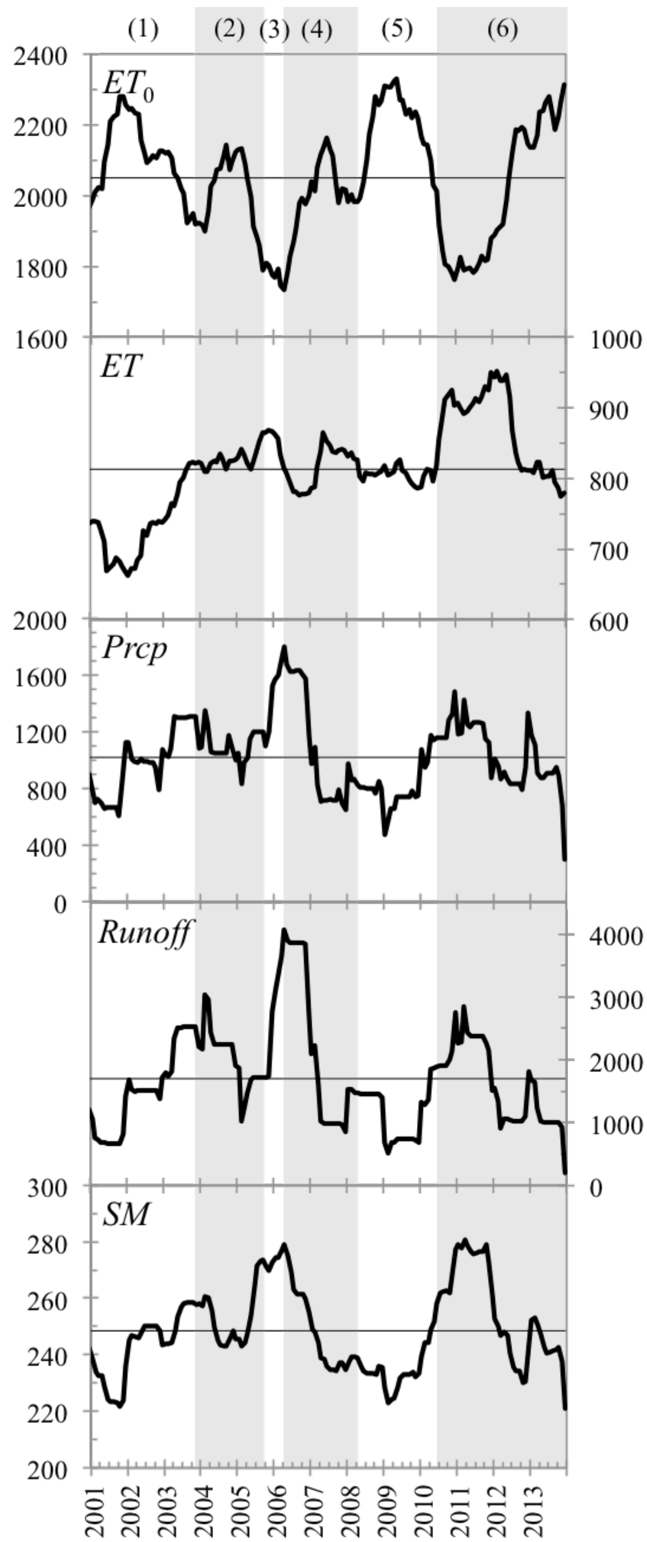

Figure 4: Linkages between areally averaged simulated water balance components. Time-series of basinwide variations in ET_0, ET, Runoff, Prcp, and SM for the Russian River basin (CA) from January, 2010, to December, 2013, with each series mean shown as a horizontal line. Units for ET_0, ET, Prcp, and Runoff are mm year^{-1}; units for SM are mm. Numbered shaded periods denote periods discussed in the text.

Figure 5
Click here to download Rendered Figure: EDDI_Part_I_Hobbins_et_al - figure 5.pdf

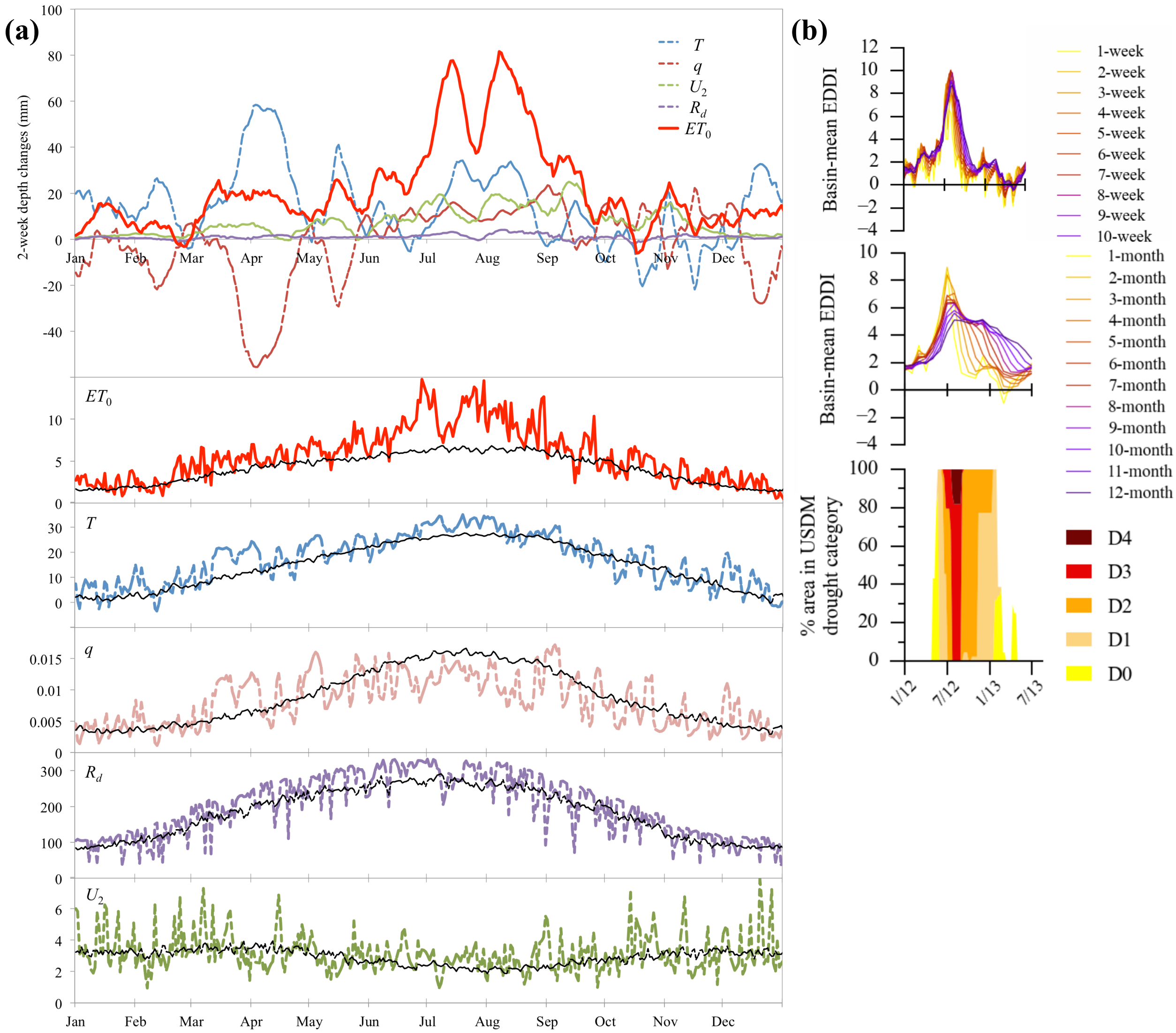

Figure 5: Example of time variations of ΔET_0 and its drivers under a flash drought during the spring and summer of 2012, in the Current River basin (MO). In **(a)** the top panel shows 2-week time series of ΔET_0 (mm) and each driver's contributions to ΔET_0 (mm); lower panels show daily time series of ET_0 (mm d^{-1}), T_{air} (^{o}C), q (kg kg^{-1}), R_d (W m^{-2}), and U_2 (m s^{-1}), respectively, with daily climatological (1981-2010) mean values in black. In **(b)** the time series of drought monitors across the basin are shown for a two-year period 2012-2013 including the flash drought: 1- to 12-weekly EDDI in the top panel; 1- to 12-monthly EDDI in the middle panel; weekly USDM plotted as percentage of basin in each USDM drought category in the bottom panel (the full time series is shown in Figure 7).

Figure 6

Click here to download Rendered Figure: EDDI_Part_I_Hobbins_et_al - figure 6.pdf

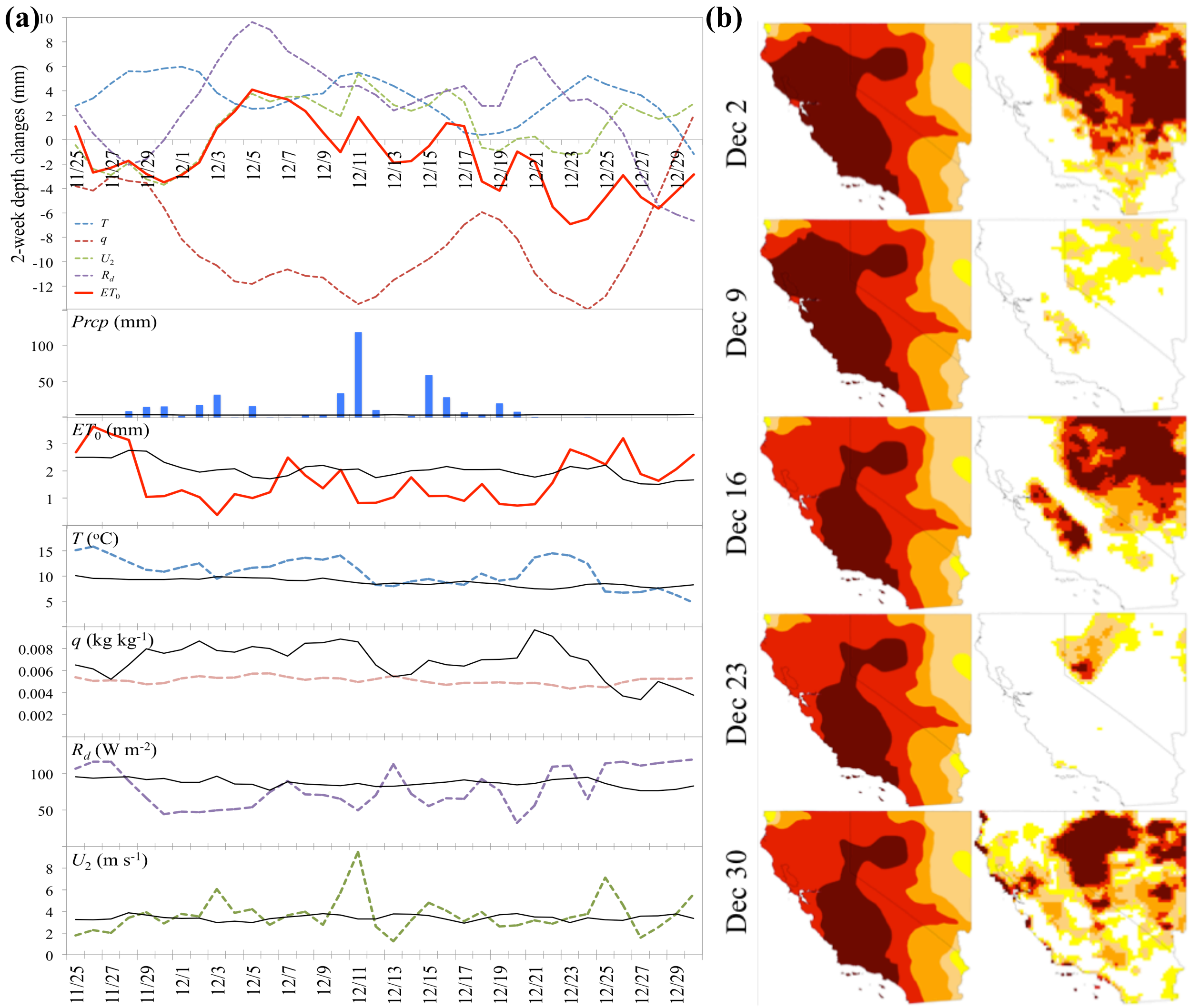

Figure 6: Example of time variations of ΔET_0 and its drivers under an intra-drought wetting interval (the landfall of an atmospheric river) from November 28 to December 21, 2014, in the Russian River basin (CA). In **(a)** the top panel shows 1-week time series of ΔET_0 (mm) and each driver's contributions to ΔET_0 (mm); lower panels show, in descending order, daily time series of Prcp (mm, recorded at the Santa Rosa, CA, weather station 047965, located within the basin), ET_0 (mm), T_{air} (°C), q (kg kg^{-1}), R_d (W m^{-2}), and U_2 (m s^{-1}), with daily climatological (1981-2010) mean values in black. In **(b)** the progression of drought monitors is mapped across CA and NV for the same period: USDM on left; 1-week EDDI on right.

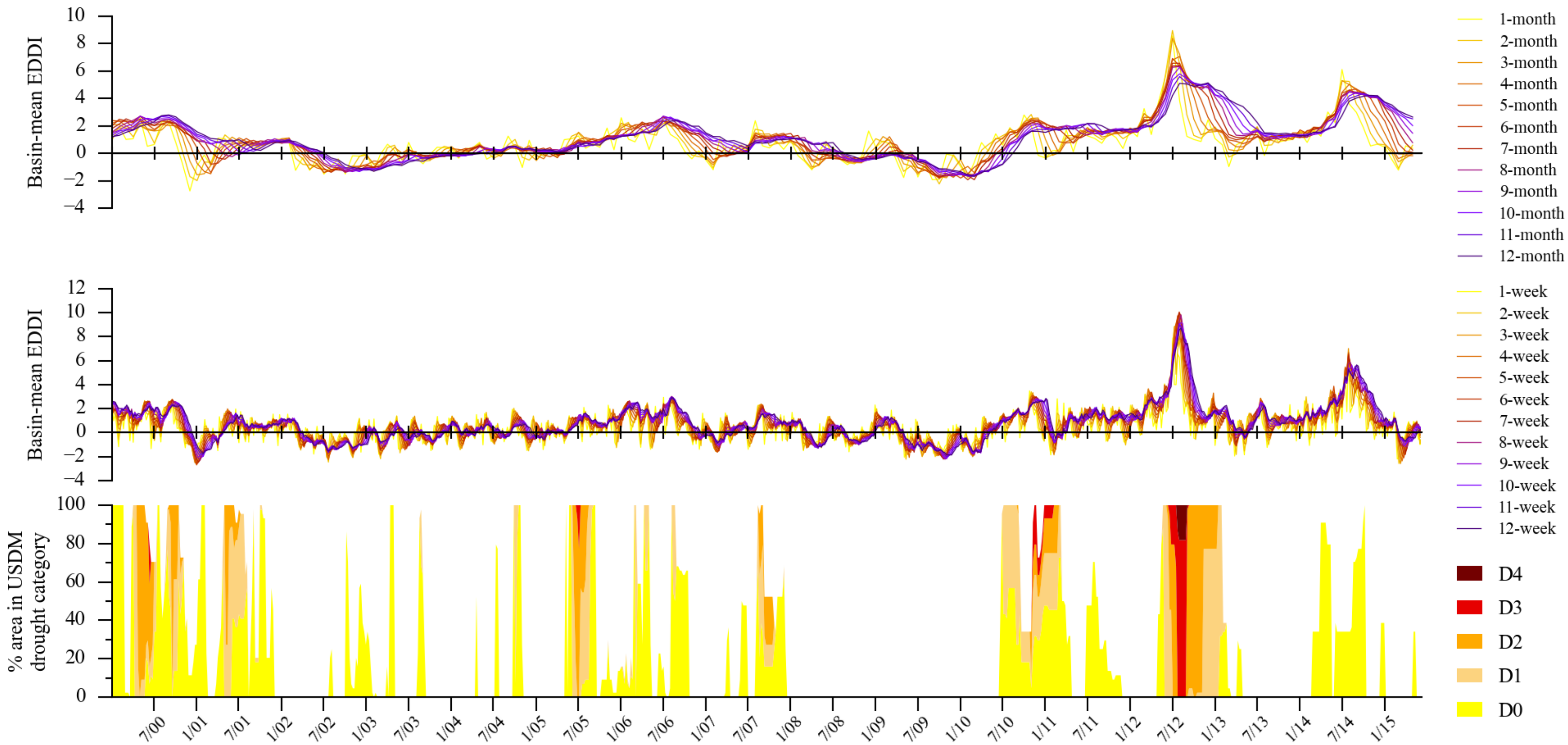

Figure 7: Basinwide time variations of multi-weekly and multi-monthly EDDI and USDM for the entire USDM period (from January 4, 2000 to the present) across the Current River basin (MO). **(Top)** is for one- to 12-monthly EDDI; **(middle)** is for the one- to 12-weekly EDDI; **(bottom)** is for weekly USDM.

Figure 8
Click here to download Rendered Figure: EDDI_Part_I_Hobbins_et_al - figure 8.pdf

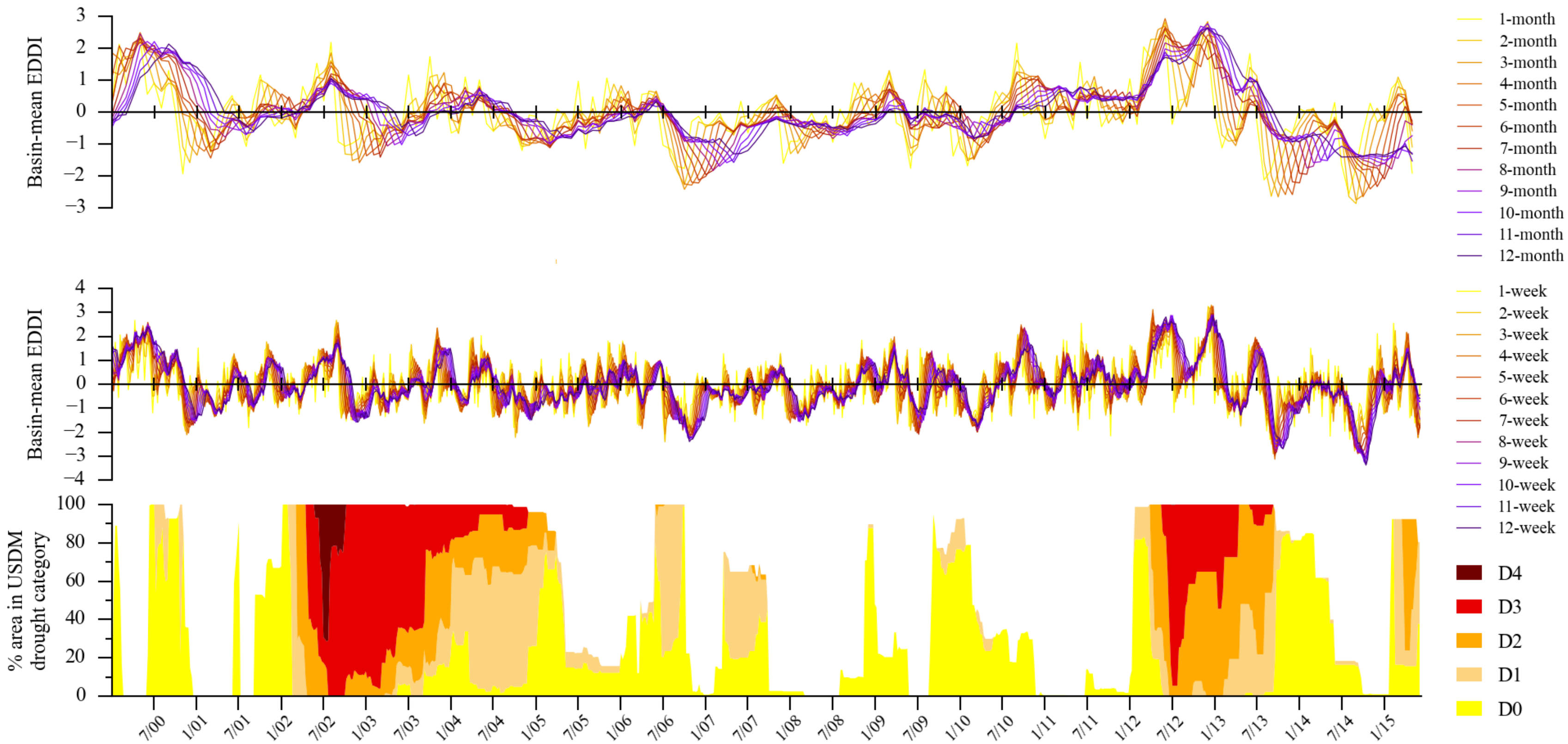

Figure 8: Basinwide time variations of multi-weekly and multi-monthly EDDI and USDM for the entire USDM period (from January 4, 2000 to the present) across the Upper Colorado River basin. **(Top)** is for one- to 12-monthly EDDI; **(middle)** is for the one- to 12-weekly EDDI; **(bottom)** is for weekly USDM.

Figure 9
Click here to download Rendered Figure: EDDI_Part_I_Hobbins_et_al - figure 9.pdf

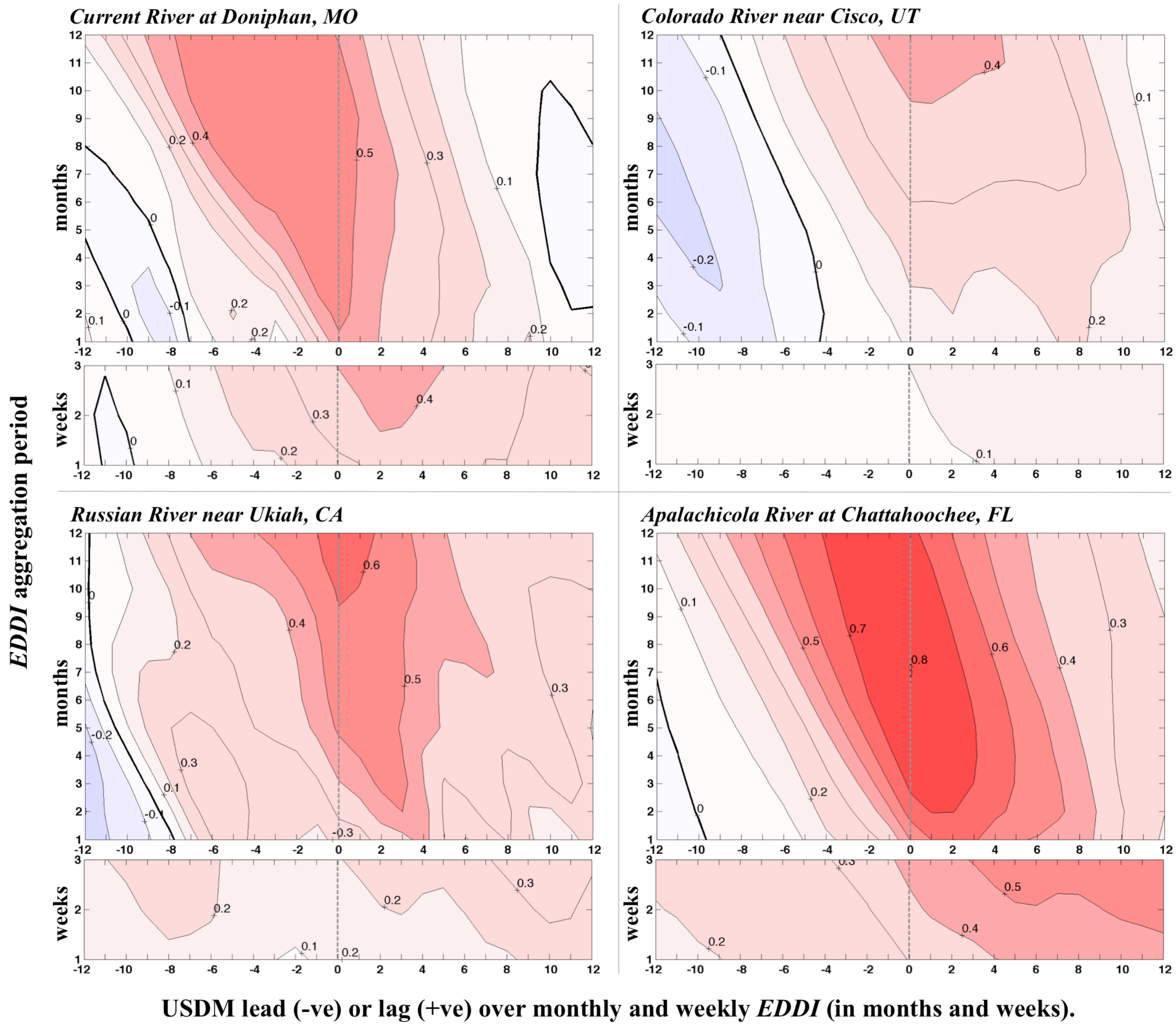

Figure 9: Correlations between river basin spatial means of USDM and EDDI. EDDI varies from 1- to 3-week and 1- to 12-month aggregation periods shown on the ordinate axes, with lead (lag) times between USDM and EDDI of up to +/- 12 weeks and months (for weekly and monthly EDDI, respectively), shown on the abscissae. Correlations are indicated by color: red positive; blue negative.

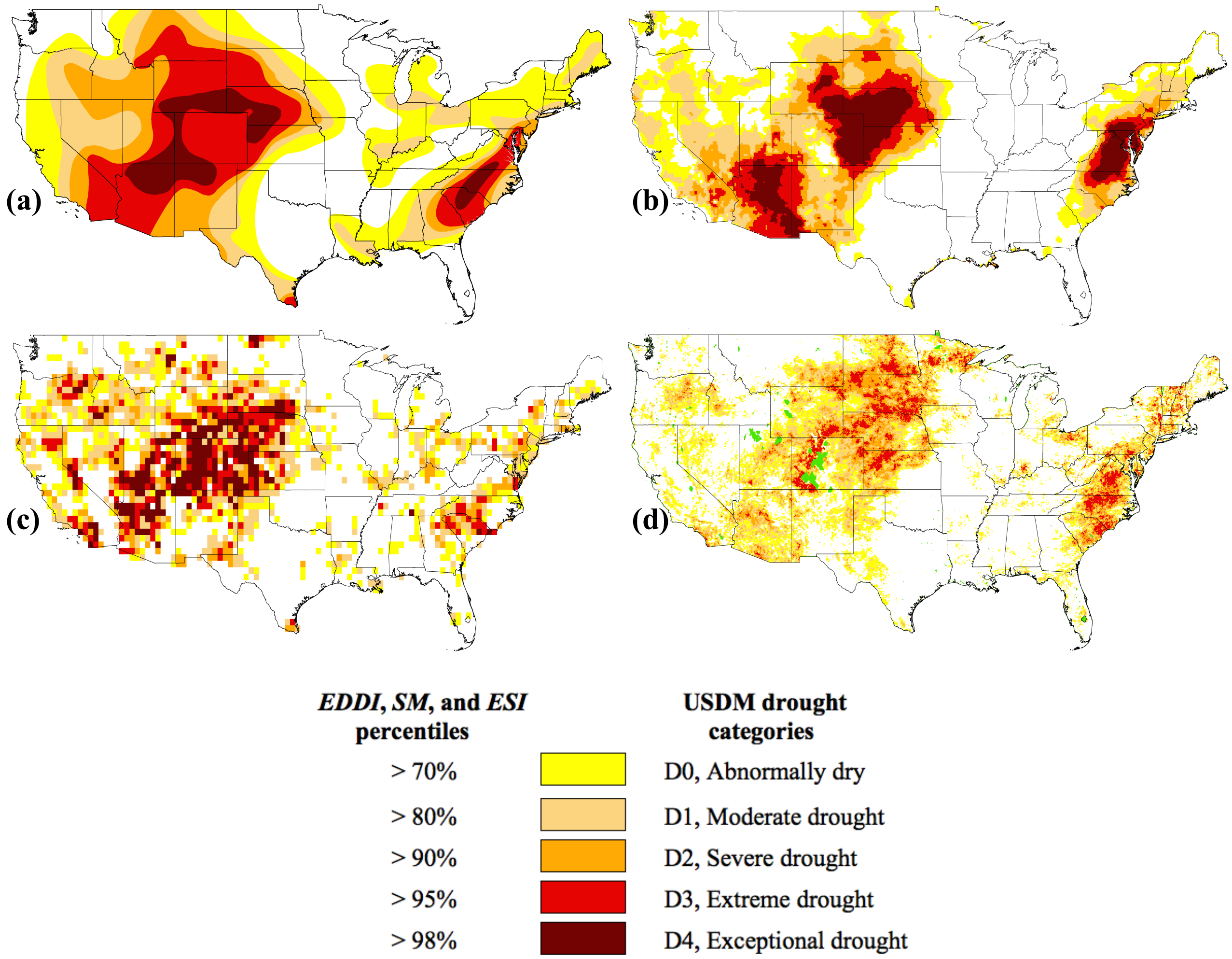

Figure 10: Comparing representations of drought conditions of mid-summer, 2002: **(a)** the USDM on July 30, 2002; **(b)** the three-month EDDI on July 31, 2002; **(c)** percentiles of VIC-modeled soil moisture (SM) from the University of Washington Surface Water Monitor (Wood 2008) on July 31, 2002; and **(d)** 12-week ESI (Anderson et al. 2007) on July 29, 2002.